

DEC 18 1977

Item 830-4-15

NAS 1.60:1077

NASA Technical Paper 1077

COMPLETED
ORIGINAL

**Sea-Surface Temperature
and Salinity Mapping
From Remote Microwave
Radiometric Measurements
of Brightness Temperature**

Hans-Juergen C. Blume, Bruce M. Kendall,
and John C. Fedors

DECEMBER 1977

NASA

29

NASA Technical Paper 1077

**Sea-Surface Temperature
and Salinity Mapping
From Remote Microwave
Radiometric Measurements
of Brightness Temperature**

**Hans-Juergen C. Blume, Bruce M. Kendall,
and John C. Fedors**

**Langley Research Center
Hampton, Virginia**



**National Aeronautics
and Space Administration**

**Scientific and Technical
Information Office**

1977

SUMMARY

A technique to measure remotely sea-surface temperature and salinity was demonstrated with a dual-frequency microwave radiometer system. Accuracies in temperature of 1°C and in salinity of 1 part per thousand (‰) for salinity greater than 5 ‰ were attained after correcting for the influence of extra-terrestrial background radiation, atmospheric radiation and attenuation, sea-surface roughness, and antenna beamwidth. The radiometers, operating at 1.43 and 2.65 GHz, comprise a third-generation system using null balancing and feedback noise injection. Flight measurements from an aircraft at an altitude of 1.4 km over the lower Chesapeake Bay and coastal areas of the Atlantic Ocean resulted in contour maps of sea-surface temperature and salinity with a spatial resolution of 0.5 km.

INTRODUCTION

Measurements of ocean temperature and salinity are useful for studying the circulation in bay areas and tracing river outflow. In particular, estuaries, as described by Thomann (ref. 1), are areas of considerable dynamic change in water temperature and salinity, being areas of mixing between fresh and ocean water. A disturbance of the status quo, caused for example by hurricanes, droughts, or extreme hot or cold spells, can cause severe stress on estuarine inhabitants (ref. 1). Also, maps of ocean temperature are useful for tracing current systems such as the Gulf Stream. Some ocean fish tend to swim along oceanic isotherms at certain times, so that a knowledge of temperature can assist in their location.

Because the microwave emission of ocean water is dependent on temperature and salinity (ref. 1), it is possible to utilize microwave radiometers to sense sea-surface temperature and salinity remotely. The emission is more dependent on salinity at lower microwave frequencies and more dependent on temperature at higher microwave frequencies. Thus, a system comprising two microwave radiometers operating at 1.43 and 2.65 GHz can provide remote measurement of both parameters. The use of a dual-frequency microwave radiometer system has an advantage over other types of remote sensing instruments in that it can operate at night and probe through clouds. Previously reported (ref. 2) measurements of salinity, obtained with a single-frequency microwave radiometer, had a root-mean-square accuracy of 2 to 3 ‰ ; however, low-altitude measurements with an infrared radiometer were required to obtain sea-surface temperature.

In this report, a dual-frequency microwave radiometer system is described along with the necessary corrections to the radiometer apparent temperature for various atmospheric and sea-surface effects. Although these corrections are small, they are necessary for accurate inversion of the measurements to obtain sea-surface temperature and salinity to the desired accuracy of 1°C and 1 ‰ .

Inversion algorithms developed for this purpose were used to produce contour maps of these quantities.

SYMBOLS

e	emissivity at nadir of calm sea surface, dimensionless
$e(\theta, T_s)$	emissivity of sea at molecular temperature T_s for viewing angle θ , dimensionless
e_λ	emissivity at wavelength λ , dimensionless
F	values of sea-surface temperature or salinity
f	frequency, GHz
h	aircraft measurement altitude, km
$P(\phi)$	antenna power pattern, dimensionless
S	salinity, parts per thousand ($^{\circ}/_{\text{oo}}$)
$\langle T \rangle$	average physical temperature of intervening atmosphere, K
T_a	equivalent antenna temperature, K
T_{atm}	terrestrial sky brightness temperature at viewing angle θ , K
T_B	sea-surface brightness temperature, K
T_C	total extraterrestrial background radiation temperature, K
T_{cos}	thermal component of cosmic background radiation, K
T_{gal}	galactic noise temperature, K
$T_o(h)$	equivalent atmospheric noise temperature at altitude h , K
T_R	radiometer apparent temperature, K
$\langle T_R \rangle$	average apparent temperature, K
T_s	sea-surface molecular temperature, K
$T(z, \theta)$	atmospheric physical temperature at altitudes z and viewing angle θ , K
ΔT_{cor}	total correction to radiometer apparent temperature, K
ΔT_p	antenna pattern temperature correction, K

ΔT_w	sea-surface roughness temperature correction, K
w	wind speed, m/sec
X_i	regression coefficients (see eq. (23))
z	altitude, km
α	atmospheric absorption coefficient, dimensionless
$\eta(\phi_1)$	antenna beam efficiency at ϕ_1 , dimensionless
θ	viewing angle from nadir, rad
λ	wavelength, cm
$\tau(h)$	atmospheric opacity at altitude h , dimensionless
τ_0	total one-way atmospheric opacity, dimensionless
$\tau(z)$	atmospheric opacity at altitude z , dimensionless
ϕ	antenna pattern angle from nadir, rad
ϕ_1	antenna half-beamwidth for 98-percent beam efficiency, rad

Superscripts:

L	1.43 GHz or L-band
S	2.65 GHz or S-band

DESCRIPTION OF RADIOMETER SYSTEM

The L-band (1.43 GHz) and S-band (2.65 GHz) radiometers used in this investigation are third-generation, advanced, switched radiometers. The design of these radiometers is based on the application of two concepts (ref. 3) to the switched-input-type receiver introduced by Dicke (ref. 4). The first concept is to equalize the temperature of the reference noise source at the circulator switch with the temperature of the lossy microwave components between the antenna terminal and the receiver input. This temperature is maintained extremely constant (± 0.03 K). The second concept is to use a feedback loop to inject pulsed portions of a constant noise source (avalanche diode) into the received noise power at the antenna terminals to equalize the noise power at both inputs of the circulator switch. The pulse frequency, which determines the average value of injected noise power, is a measure of the noise power (radiation) received by the antenna. As a result of these two design improvements, the radiometers are nearly independent of gain variations and errors that are contributed by front-end losses. The radiometers therefore exhibit the long-term stability that is necessary to achieve absolute brightness temperature measurements to within a few tenths kelvin. The stability also eliminates the need for periodic calibra-

tion cycles and the resulting loss of data. The S-band radiometer, described in detail in reference 3, has a superheterodyne receiver. The L-band radiometer, developed at the NASA Langley Research Center, is similar to the S-band radiometer except that the L-band radiometer has a direct-type receiver; that is, it has no mixer and intermediate-frequency (IF) section.

A simplified block diagram of the radiometer system is shown in figure 1. The radiation received by the antenna has the injected noise added to it. The circulator switch then switches between this sum of noise power and that of the matched termination which is at the reference temperature. The circulator switch output is amplified by the receiver's low-noise parametric amplifier and detected by a square-law detector. The detector output is demodulated in synchronism with the circulator switch to produce a voltage driving the voltage-to-frequency converter. The output signal from the voltage-to-frequency converter is used to gate the noise injection pulse driver which adjusts the injected noise power level to achieve a null at the output. Gating the noise source with constant-width pulses produces a linear relationship between the pulse frequency and the average injected noise. It is this linearity that allows accurate measurement over a wide range of brightness temperatures (typically 303 K). Finally the output data are recorded in digital form on magnetic tape and in analogue form on a strip-chart recorder. In both cases, even slight variations in the reference temperature are recorded for correction of the output data. The S-band and L-band radiometers have resolutions of ± 0.08 K and ± 0.09 K, respectively, and with suitable calibration, both have an absolute accuracy of better than ± 0.2 K.

The output data of both radiometers are converted to digital form by a data processor developed at the NASA Langley Research Center. The processor also conditions and formats the housekeeping data from other sources that are necessary for the reduction of the radiometric data, such as flight parameters, time, latitude, and longitude. The data recorded on digital magnetic tape are also displayed as L-band and S-band radiometer apparent temperature by the data processor. The data processor is capable of adjusting measurement integration times independent of the radiometer settings. This capability provides an efficient way to adapt the overall integration time to the aircraft altitude and measurement spatial resolution (antenna half-power footprint size).

MICROWAVE BRIGHTNESS TEMPERATURE OF THE SEA

Quantitative measurements of the thermal emission from the sea surface require corrections for the radiative and transmissive properties of the intervening atmosphere and sky, antenna beam efficiency, and sea-surface roughness. At the measurement wavelengths of 11 and 21 cm, there are four principal atmospheric and sky effects which must be considered:

- (1) Cosmic background radiation
- (2) Radiation from galactic and discrete celestial radio sources

(3) Attenuation from oxygen and water vapor

(4) Radiation from the Sun

It has long been known that the Earth's atmosphere is essentially transparent to transmission of electromagnetic radiation at frequencies of 1 to 3 GHz. Extensive work over the years on microwave signal propagation through the atmosphere at centimeter wavelengths has indicated that the influence of clouds is small at these frequencies except under very severe storm conditions. An added factor for consideration is that the background galactic noise tends to decrease substantially as frequencies increase beyond about 1 GHz. Therefore, the frequency regime from 1 to 3 GHz is a well-suited choice for minimizing the effects of extraterrestrial background radiation and atmospheric interference.

Despite these advantages, accurate surface temperature measurement by airborne radiometers in this microwave region requires detailed knowledge of these effects for correcting the instrumental observations. The corrections to the measured brightness temperature of the ocean surface can still be of the order of a few kelvins and therefore, must be taken into account. The apparent temperature T_R (which may also be called the equivalent radiometric temperature of the complete set of received radiations) is calculated from the equation of radiative transfer by making use of the Rayleigh-Jeans approximation to the Planck law:

$$\begin{aligned} T_R(\theta) = & \left\{ 1 - e(\theta, T_S) \right\} \left\{ T_C \exp \left[- \int_0^\infty \alpha(\theta, z) dz \right] \right. \\ & + \left. \int_0^\infty T(z, \theta) \exp \left[- \int_0^z \alpha(\theta, z) dz \right] \alpha(\theta, z) dz \right\} \exp \left[- \int_0^h \alpha(\theta, z) dz \right] \\ & + e(\theta, T_S) T_S \exp \left[- \int_0^h \alpha(\theta, z) dz \right] + \int_0^h T(z, \theta) \exp \left[- \int_0^z \alpha(\theta, z) dz \right] \alpha(\theta, z) dz \end{aligned} \quad (1)$$

where

$e(\theta, T_S)$ emissivity of sea at molecular temperature T_S for nadir viewing angle θ

h altitude of aircraft

T_C total extraterrestrial background radiation temperature

$T(z, \theta)$ temperature of atmosphere at altitudes z and viewing angle θ

$\alpha(\theta, z)$ atmospheric absorption coefficient at z and θ

The first term in equation (1) comprises the temperature of the downward radiation of the extraterrestrial noise, attenuated by the entire atmosphere, and the

downward radiation of the atmosphere itself, reflected by the ocean surface and in turn attenuated by the intervening atmosphere between the ocean and radiometer. The second term accounts for the attenuated emission from the ocean surface. The third term accounts for the upward emission of the atmosphere between the ocean and the radiometer.

Since the antenna gain pattern for most radiometers is highly directional and falls off rapidly with increasing θ , a horizontally stratified atmosphere model can be used to approximate equation (1) by replacing the nested integrals with opacities:

$$T_R(\theta) = \{1 - e(\theta, T_S)\} \left\{ T_C \exp[-\tau_0 \sec \theta] + \int_0^\infty T(z) \exp[-\tau(z) \sec \theta] \alpha(z) \sec \theta dz \right\} \exp[-\tau(h) \sec \theta] + e(\theta, T_S) T_S \exp[-\tau(h) \sec \theta] + \int_0^h T(z) \exp[-\tau(z) \sec \theta] \alpha(z) \sec \theta dz \quad (2)$$

where τ_0 is the total one-way opacity of the atmosphere and $\tau(h)$ and $\tau(z)$ are the opacities at altitudes h and z .

The extraterrestrial background radiation (T_C) consists of galactic noise (T_{gal}), the thermal component of cosmic background radiation (T_{cos}), and emission from strong radio sources such as the Sun. Since the Sun is a point source, its contribution depends strongly on the antenna viewing angle, the Sun's position, the antenna pattern, and the roughness of the sea surface. However, as explained subsequently, the Sun's contribution was considered to be negligible. Therefore,

$$T_C = T_{cos} + T_{gal} \quad (3)$$

The galactic radiation component includes only that portion of the galactic radiation entering vertically into the measurement area. The galactic sector 6 hours to 9 hours right ascension and 27° to 47° declination was overhead during the time of measurement and within the 20° antenna beam coverage. The thermal contribution of the galaxy is determined by a curve-fitting method suggested in reference 5. The equivalent exo-atmospheric temperature in kelvins of the galactic radiation from the specified galactic sector during the measurement period is

$$T_{gal} = 2.34f^{-2.53} \quad (4)$$

where f is the frequency in GHz. The cosmic background radiation T_{cos} is frequency independent over the microwave band (ref. 6) and is equal to 2.7 K.

For the clear atmosphere, water vapor and molecular oxygen are the major sources of attenuation in the microwave region. At frequencies of 1.43 and 2.65 GHz, attenuation due to water vapor is about an order of magnitude less than that due to molecular oxygen. Since the total opacity of the atmosphere is only of the order of 0.01, it is sufficient to consider the absorption due to molecular oxygen alone. The brightness temperature T_{atm} of the terrestrial sky at zenith angle θ is

$$\int_0^\infty T(z) \exp [-\tau(z) \sec \theta] \alpha(z) \sec \theta \, dz \quad (5)$$

which contains the atmospheric term of equation (2). It has been measured for the clear atmosphere at 2.65 GHz (ref. 7). These observations indicated that the zenith brightness temperature and, therefore, the opacity of the cloudless terrestrial sky, are consistent with the predictions of the Van Vleck-Weisskopf model for oxygen absorption. The measurements at 2.65 GHz give 2.2 K for the zenith sky temperature and a value for τ_0 of 0.0091. For 1.43 GHz, the theory predicts values of 2.1 K and 0.008 for T_{atm} and τ_0 , respectively. The term $e(\theta, T_s) T_s$ of equation (2) may be replaced by the sea-surface brightness temperature T_B .

Because τ_0 and $\tau(h)$ are very small, the exponential terms of equation (2) may be approximated by

$$\exp [-\tau \sec \theta] = 1 - \tau \sec \theta \quad (6)$$

Also, by considering that the measurements of this investigation were taken along the nadir (i.e., $\theta = 0$), $\sec \theta$ in equation (6) can be set to unity. A further simplification is made by evaluating the one-way opacity between the sea surface and the radiometer antenna as

$$\tau(h) = \int_0^h \alpha(z) \, dz \quad (7)$$

and the equivalent noise temperature of the intervening atmosphere as

$$T_0(h) = \int_0^h T(z) \exp [-\tau(z)] \alpha(z) \, dz \quad (8)$$

Equation (8) is the last term of equation (2) with $\sec \theta = 1$. The atmospheric opacity or attenuation $\tau(h)$ and equivalent noise temperature $T_0(h)$ of the 1962 U.S. Standard Atmosphere at 1.43 and 2.65 GHz for different altitudes are shown in figure 2. Figure 2 also shows that at altitudes less than 2 km, the opacity $\tau(h)$ is approximately linear with altitude, having values of approximately 0.00136h and 0.00154h at 1.43 and 2.65 GHz, respectively. The right side of equation (8) can (for $h < 2.5$ km) be approximated by $\langle T \rangle \tau(h)$ where $\langle T \rangle$ is the averaged physical temperature of the intervening atmosphere between the radiometer and the sea surface.

By applying the preceding approximations and derivations and replacing the term $e(\theta, T_s)$ with e (the nadir emissivity of the calm sea surface), equation (2) simplifies to

$$T_R = T_B[1 - \tau(h)] + (1 - e)[1 - \tau(h)] [(T_{cos} + T_{gal})(1 - \tau_0) + T_{atm}] + \tau(h) \langle T \rangle \quad (9)$$

Unless the sea surface is perfectly smooth (no waves), a surface roughness correction (ΔT_w) is necessary at some microwave frequencies because of the dependence of emissivity on roughness. For the exact measurement of the apparent temperature, the antenna should have a "pencil" beam pattern. Since this is impossible to achieve, an antenna pattern correction (ΔT_p) must be made (ref. 8). Adding these two additional corrections to equation (9) results in

$$T_R = T_B [1 - \tau(h)] + (1 - e) [1 - \tau(h)] [(T_{cos} + T_{gal})(1 - \tau_o) + T_{atm}] + \tau(h) \langle T \rangle + \Delta T_w + \Delta T_p \quad (10)$$

The sea-surface roughness can be expressed in terms of wind speed w . On the basis of prior flight data obtained with the S-band radiometer (ref. 9), the wind speed correction at 2.65 GHz was found to be $0.56w^{0.53}$. No correction for surface roughness due to wind speed at 1.43 GHz is included because recent data indicate that it is negligible at this frequency (ref. 10).

The antenna pattern correction is obtained by evaluation of the antenna temperature integrals (ref. 9),

$$T_a = \frac{\int_0^{\phi_1} T_R(\phi) P(\phi) \sin \phi d\phi}{\int_0^\pi P(\phi) \sin \phi d\phi} + \frac{\int_{\phi_1}^\pi T_R(\phi) P(\phi) \sin \phi d\phi}{\int_0^\pi P(\phi) \sin \phi d\phi} \quad (11)$$

where the antenna temperature T_a is the equivalent temperature of the radiation incident within the antenna beamwidth ($2\phi_1$) plus the radiation incident outside this beamwidth, $T_R(\phi)$ is the apparent temperature of the sea surface in the direction ϕ from the nadir, and $P(\phi)$ is the antenna power pattern. The antenna beamwidth $2\phi_1$ for a 98-percent antenna beam efficiency was 50° in this case. The first term in equation (11) is by definition the antenna beam efficiency $\eta(\phi_1)$. For antennas with high beam efficiencies, such as those of the L- and S-band radiometer system, equation (11) may be approximated by

$$T_a = \eta(\phi_1) T_R + [1 - \eta(\phi_1)] \langle T_R \rangle \quad (12)$$

where $\langle T_R \rangle$ is the average apparent temperature from radiation present outside the antenna beamwidth. The antenna pattern correction is then

$$\Delta T_p = T_a - T_R = [1 - \eta(\phi_1)] [\langle T_R \rangle - T_R] \quad (13)$$

Evaluation of equation (13) for the 2.65-GHz antenna is described in detail in reference 9 and was found to yield 0.4 K. A similar evaluation was performed with the aid of the 1.43-GHz antenna patterns shown in reference 11 and resulted in an antenna pattern correction of 0.14 K.

The results of evaluation of all unwanted contributions to the observed temperature (radiometer apparent temperature) are listed in table I for both frequencies. Using these results in equation (10) gives

$$T_R^S = T_B^S [1 - \tau^S(h)] + [1 - e^S] [1 - \tau^S(h)] 5.1 + \tau^S(h) \langle T \rangle + 0.56w^{0.53} + 0.4 \quad (14)$$

$$T_R^L = T_B^L [1 - \tau^L(h)] + [1 - e^L] [1 - \tau^L(h)] 5.8 + \tau^L(h) \langle T \rangle + 0.14 \quad (15)$$

where the superscripts S and L refer to 2.65 GHz and 1.43 GHz, respectively, T_R^S and T_R^L are the respective radiometer apparent temperatures, h is the aircraft altitude in kilometers, and w the wind speed in meters/second. Equations (14) and (15) may be used without affecting the measurement accuracy if

(1) measurement is in nadir direction, (2) there is no precipitation, (3) the radiometers are operated at microwave frequencies lower than 3 GHz, (4) the altitude of the radiometers is low (less than 2.5 km), and (5) the Sun is low in the sky (i.e., negligible Sun contribution).

Rearranging equations (14) and (15) gives

$$T_R^S = [1 - \tau^S(h)] [T_B^S + 5.1(1 - e^S)] + \tau^S(h) \langle T \rangle + 0.56w^{0.53} + 0.4 \quad (16)$$

$$T_R^L = [1 - \tau^L(h)] [T_B^L + 5.8(1 - e^L)] + \tau^L(h) \langle T \rangle + 0.14 \quad (17)$$

Because the terms $5.1(1 - e^S)$ and $5.8(1 - e^L)$ are always small in comparison with T_B^S and T_B^L , the $(1 - e)$ terms may be approximated by the constant value of 0.65 since the emissivity e is close to 0.35. Hence,

$$T_R^S = T_B^S + 3.7 + \tau^S(h) [\langle T \rangle - T_B^S - 3.3] + 0.56w^{0.53} \quad (18)$$

$$T_R^L = T_B^L + 3.9 + \tau^L(h) [\langle T \rangle - T_B^L - 3.8] \quad (19)$$

Within the bracket term only, $\langle T \rangle$, T_B^S , and T_B^L may normally be approximated by 283 K, 105 K, and 95 K, respectively.

Using the expressions listed in table I for $\tau^S(h)$ and $\tau^L(h)$ and solving for the brightness temperature of the sea surface T_B result in the following two equations:

$$T_B^S = T_R^S - 3.7 - 0.269h - 0.56w^{0.53} \quad (20)$$

$$T_B^L = T_R^L - 3.9 - 0.251h \quad (21)$$

DETERMINATION OF SALINITY AND SURFACE TEMPERATURE FROM MICROWAVE BRIGHTNESS TEMPERATURE

The brightness temperature T_B measured by an ideal radiometer is related to the molecular temperature of a radiating surface via the emissivity of the surface. The emissivity of a dielectric surface at a particular wavelength is determined by its complex dielectric constant which for sea water is a function only of temperature and salinity. Therefore, the brightness temperature of the sea surface is given by

$$T_B(\lambda) = e_\lambda(T_s, S) T_s \quad (22)$$

where the emissivity e at the wavelength λ is expressed in terms of surface temperature T_s and salinity S . Plots of brightness temperature as a function of salinity and surface temperature at 1.43 GHz and 2.65 GHz are given in figures 3 and 4, respectively (ref. 12). These plots were basically derived from experimental measurements of the dielectric constant of sea water at 1.43 GHz

(ref. 13) with a few experimental errors removed by utilizing data obtained previously at 2.65 GHz (ref. 14). The frequency dependency was accounted for by means of the Debye equation (ref. 15). The values on which the family of curves are based have published accuracies (ref. 12) of 1 ‰ for salinity (S greater than 5 ‰) and 0.5° C for sea-surface temperature.

In order to invert the brightness temperatures T_B^S and T_B^L in figures 3 and 4 to corresponding values of T_S and S , the following regression equation was developed:

$$F = X_1 T_B^S + X_2 T_B^L + X_3 T_B^S T_B^L + X_4 (T_B^S)^2 + X_5 (T_B^L)^2 + X_6 (T_B^S)^3 + X_7 (T_B^S)^2 T_B^L + X_8 T_B^S (T_B^L)^2 + X_9 (T_B^L)^3 \quad (23)$$

where F is equal to either T_S or S depending on the set of regression coefficients X_i (listed in table II) used.

The regression coefficients were found from input data consisting of two 9 by 9 tables of brightness temperature as a function of salinity and molecular surface temperature; one table was for 2.65 GHz and the other for 1.43 GHz. The coefficients X_i were computed so that the mean-square error between input salinity or temperature and the corresponding quantity computed from equation (23) was minimized over the input data set.

FLIGHT OBSERVATIONS AND COMPARISON WITH SEA-TRUTH DATA

On August 24, 1976, the L- and S-band radiometer system was installed on a NASA C-54 aircraft, and a functional check-out flight was conducted from the NASA Wallops Flight Center over the lower part of the Chesapeake Bay and adjacent Atlantic Ocean. A flight over the entrance to the Chesapeake Bay was selected because the mixing of fresh and salt water there should result in high salinity gradients, and instrument performance could therefore be verified over a wide range of salinity concentration. The results are reported in the form of synoptic maps of salinity and temperature, and the data are compared with sea-truth measurements. These sea-truth measurements were obtained via the bucket method: water temperature of bucket samples taken at the surface was measured with a thermometer, and samples of the same water were analyzed in a laboratory for salinity using the silver nitrate technique. The accuracy of the sea-truth measurements was about 0.1 ‰ for salinity and about 0.1° C for water temperature.

Sea conditions for the measurement were fairly calm with a 3.5-m/sec surface wind. During the test flight, the data were taken under cloudless but hazy atmospheric conditions with the aircraft in level flight (roll and pitch less than 2°) at an altitude of 1.4 km, so that all the measurements refer to observations at nadir. During the measurement time period between 9:00 a.m. and 12:00 p.m. EST, the elevation angle of the Sun varied from 41° to 64°, so that there was no Sun contribution to the nadir microwave measurements. The spatial resolution of the measurement, or antenna half-power footprint size, was 0.5 km. Introducing these parameters into equations (20) and (21) results in

$$T_B^S = T_R^S - 5.2 \quad (24)$$

and

$$T_B^L = T_R^L - 4.2 \quad (25)$$

where T_B^S and T_B^L are in kelvins.

Both radiometers were calibrated before the flight by using a specially designed liquid-nitrogen cryogenic antenna load (ref. 16) placed under and closely coupled to the antenna. This calibration procedure is reported for the S-band radiometer in reference 9. Since all the corrections that were applied in deriving equations (24) and (25) were to some degree inaccurate and there were some inaccuracies associated with the radiometers in the measurement of microwave brightness temperature, an error budget has been prepared. Table III lists the possible errors in terms of radiometric brightness temperature for each radiometer due to atmospheric and sky emission effects, antenna beam efficiency correction, calibration, and instrument stability. Included also is the temperature resolution (i.e., relative accuracy) for a 1-second integration time and 100-MHz bandwidth for the S-band radiometer and 60-MHz bandwidth for the L-band radiometer.

The measured radiometric data, together with latitude and longitude coordinates from the aircraft's inertial navigation system, were recorded on digital magnetic tape and computer processed according to equations (23), (24), and (25). The sea-truth data were obtained within 30 minutes of the radiometric data from several locations in the measurement area. These locations and the flight lines used to obtain the radiometric data are shown in figure 5. Although it had been planned to have the sea-truth locations correspond to the flight lines, an accumulative drift of about 0.2 minute in latitude per flight line in the inertial navigation system during the measurement prevented this. A sample section of the raw analogue data taken along the first flight line (37°16' latitude) and over sea-truth location 1 is shown in figure 6. The fluctuations of T_R^S and T_R^L around the mean values represent the fine structure of salinity and temperature variations, since the brightness temperature resolutions of both radiometers are less than 0.1 K. It is obvious from the data traces that T_R^L is much more responsive to salinity gradients between the Chesapeake Bay and the Atlantic Ocean than T_R^S . The necessary corrections ΔT_{cor}^S and ΔT_{cor}^L listed in table I and incorporated in equations (24) and (25) are indicated at sea-truth location 1. The resulting brightness temperatures T_B^S and T_B^L are converted into a salinity of 18 ‰ and a temperature of 24.6° C via the regression equation (23). These values differ from the sea-truth surface measurement by less than the target accuracy of 1 ‰ and 1° C.

A comparison of the radiometrically measured values of surface temperature and salinity with those taken at the sea-truth locations is shown in figure 7. This figure shows a section of computer-derived remote measurements as a function of latitude and longitude in the area of the surface measurements along with the values of the corresponding sea-truth data. Data points which were unusable because of radio interference from local radar or the presence of land are indicated by the symbol X. Several surface measurements were taken around sea-truth location 10 to determine variation of the sea-truth data in a given

small area. Since the flight lines did not always coincide with the sea-truth locations, a comparative analysis of the measured results with the sea-truth data required some arithmetic averaging of the measured data in the vicinity of the sea-truth locations. The values for salinity and surface temperature are compared with the corresponding sea-truth data in table IV. It should be noted that the sea-truth data shown for location 10 are mean values of the several measurements. Also, no comparison was made for location 11, as the radiometer measurements there were influenced by the presence of land. The resulting error mean deviation of -0.52 ‰ and 0.55° C and error standard deviation of 0.92 ‰ and 0.59° C for salinity and surface temperature, respectively, seem to indicate that the desired accuracy of 1 ‰ for salinity and 1° C for temperature was achieved, although only a 50-percent confidence factor can be applied to these deviations because of the small number of data points for comparison.

The calculated values of salinity and surface temperature were plotted as a function of geographic position. A contour map of the salinity distribution is shown by isohalines in 2 ‰ increments in figure 8. It can be seen from the figure that the higher salinities indeed exist in the ocean and are reduced considerably by mixing with fresh water outflow in the bay region. Evidently the ocean water with its higher salinities is pushed into the northern part of the Chesapeake Bay entrance by tidal effects and up the inside of the Delmarva Peninsula. The lower salinity bay waters flow south out the southern part of the bay entrance into the ocean, because of Coriolis forces (private communication with B. Boicourt, CBI, Johns Hopkins Univ., Baltimore, Md., 1976). A contour map of the surface temperature in 2° C increments is shown in figure 9. The cooler temperatures exist in the ocean and are influenced by the warmer temperatures of the fresh water outflow in the region of mixing. The fine structure of surface temperature caused by upwelling, heating in shallow waters by the Sun's radiation, and outflow of rivers is averaged in order to show the general temperature distribution. Again, a southern outflow of the warmer Chesapeake Bay waters is indicated.

CONCLUDING REMARKS

A dual-frequency (1.43 and 2.65 GHz) radiometer system was developed to measure salinity to 1 part per thousand (‰) (for salinity greater than 5 ‰) and sea-surface temperature to 1° C . This system utilized a null-balancing feedback circuit with noise injection for stabilization. It was operated from an aircraft over the lower Chesapeake Bay and adjacent coastal area of the Atlantic Ocean to map salinity and sea-surface temperature. To obtain the stated accuracies, the radiometer data were corrected for extraterrestrial background radiation, atmospheric effects, sea-surface roughness, and antenna beam efficiency.

Langley Research Center
National Aeronautics and Space Administration
Hampton, VA 23665
October 26, 1977

REFERENCES

1. Thomann, Gary C.: Remote Measurement of Salinity in an Estuarine Environment. *Remote Sensing Environ.*, vol. 2, no. 4, 1973, pp. 249-259.
2. Thomann, Gary C.: Experimental Results of the Remote Sensing of Sea-Surface Salinity at 21-cm Wavelength. *IEEE Trans. Geosci. Electron.*, vol. GE-14, no. 3, July 1976, pp. 198-214.
3. Hardy, Walter N.; Gray, Kenneth W.; and Love, A. W.: An S-Band Radiometer Design With High Absolute Precision. *IEEE Trans. Microwave Theory & Tech.*, vol. MTT-22, no. 4, Apr. 1974, pp. 382-390.
4. Dicke, R. H.: The Measurement of Thermal Radiation at Microwave Frequencies. *Rev. Sci. Instrum.*, vol. 17, no. 7, July 1946, pp. 268-275.
5. Apinis, John J.; and Peake, William H.: Passive Microwave Mapping of Ice Thickness. Final Rep. 3892-2 (NASA Grant NSG-3005), Ohio State Univ. Electros. Lab., Aug. 1976. (Available as NASA CR-149104.)
6. Shakeshaft, J. R.; and Webster, A. S.: Microwave Background in a Steady State Universe. *Nature*, vol. 217, no. 5125, Jan. 20, 1968, pp. 339-340.
7. Ho, W.; Wang, H. H.; Hall, W. F.; Norris, W.; Hardy, W. N.; Gray, K. W.; and Hidy, G. M.: Brightness Temperature of the Terrestrial Sky at 2.66 GHz. *J. Atmos. Sci.*, vol. 29, no. 6, Sept. 1972, pp. 1210-1212.
8. Beck, F. B.: Antenna Pattern Corrections to Microwave Radiometer Temperature Calculations. *Radio Sci.*, vol. 10, no. 10, Oct. 1975, pp. 839-845.
9. Blume, Hans-Juergen C.; Love, A. W.; Van Melle, M. J.; and Ho, William W.: Radiometric Observations of Sea Temperature at 2.65 GHz Over the Chesapeake Bay. *IEEE Trans. Antennas & Propag.*, vol. AP-25, no. 1, Jan. 1977, pp. 121-128.
10. Webster, William J., Jr.; Wilheit, Thomas T.; Ross, Duncan B.; and Gloersen, Per: Spectral Characteristics of the Microwave Emission From a Wind-Driven Foam-Covered Sea. *J. Geophys. Res.*, vol. 81, no. 18, June 20, 1976, pp. 3095-3099.
11. Bailey, M. C.: The Development of an L-Band Radiometer Dual-Mode Horn. *IEEE Trans. Antennas & Propag.*, vol. AP-23, no. 3, May 1975, pp. 439-441.
12. Klein, Lawrence A.; and Swift, Calvin T.: An Improved Model for the Dielectric Constant of Sea Water at Microwave Frequencies. *IEEE Trans. Antennas & Propag.*, vol. AP-25, no. 1, Jan. 1977, pp. 104-111.
13. Ho, W. W.; Love, A. W.; and Van Melle, M. J.: Measurements of the Dielectric Properties of Sea Water at 1.43 GHz. NASA CR-2458, 1974.

14. Ho, W.; and Hall, W. F.: Measurements of the Dielectric Properties of Seawater and NaCl Solutions at 2.65 GHz. J. Geophys. Res., vol. 78, no. 27, Sept. 20, 1973, pp. 6301-6315.
15. Grant, E. H.; Buchanan, T. J.; and Cook, H. F.: Dielectric Behavior of Water at Microwave Frequencies. J. Chem. Phys., vol. 26, no. 1, Jan. 1957, pp. 156-161.
16. Hardy, Walter N.: Precision Temperature Reference for Microwave Radiometry. IEEE Trans. Microwave Theory & Tech., vol. MTT-21, no. 3, Mar. 1973, pp. 149-150.

TABLE I.- CORRECTIONS TO RADIOMETER APPARENT TEMPERATURE AT 1.43 AND 2.65 GHz

Effect	Correction		Comments
	2.65 GHz (S-band)	1.43 GHz (L-band)	
Cosmic background radiation, T_{cos} , K	2.7	2.7	Summarized in reference 6
Galactic radiation, T_{gal} , K	0.2	1.0	Only for specified galactic quadrant according to equation (4)
Atmospheric contribution (oxygen), T_{atm} , K	2.2	2.1	Consistent with Van Vleck- Weisskopf model and 1962 U.S. Standard Atmosphere
Nonideal antenna, ΔT_p , K	0.4	0.14	Both antennas are nonscan- ning, high-beam-efficiency, multi-mode circularly polarized horns with 20° half-power beamwidth
Surface roughness, ΔT_w , K	1.1	0	S-band correction obtained experimentally; $\Delta T_w = 0.56w^{0.53}$ L-band correction negligible
Total atmospheric opacity, τ_o	0.0091	0.008	
Opacity at altitude h , $\tau(h)$	0.00154h	0.00136h	$\tau(h)$ is linear up to 2.5 km (fig. 2)
Total correction to T_R , ΔT_{cor} , K	5.2	4.2	Cumulative correction factor to the apparent tempera- ture for $w = 3.5$ m/sec and $h = 1.4$ km

TABLE II.- REGRESSION COEFFICIENTS FOR SURFACE TEMPERATURE
AND SALINITY COMPUTATION

	Regression coefficients for computation of -	
	Temperature	Salinity
X ₁	16.9073567947	138.2129737430
X ₂	-21.8805724219	-137.4748877279
X ₃	.4925788939	7.0376869542
X ₄	-.3647221634	-4.6052164921
X ₅	-.0475842615	-2.4460477714
X ₆	.0051508507	.0403065628
X ₇	-.0122197794	-.0844284343
X ₈	.0099636042	.0556040411
X ₉	-.0031929574	-.0124179422

TABLE III.- ERROR BUDGET IN MEASUREMENT OF SEA-SURFACE
BRIGHTNESS TEMPERATURE

Error source	S-band error, K	L-band error, K
Atmospheric and sky emission effects	0.3	0.3
Antenna pattern	.1	.1
Instrument calibration	.1	.1
Instrument stability	.1	.1
Temperature resolution	.08	.09
Maximum error, K	0.68	0.69
Root-mean-square error, K34	.34

TABLE IV.- COMPARISON OF RADIOMETRIC AND SEA-TRUTH MEASUREMENTS

Location no.	Salinity, ‰			Temperature, °C		
	Sea truth	Radiometric	Error ^a	Sea truth	Radiometric	Error ^a
1	17.7	18.0	-0.3	25.5	24.6	0.9
2	18.0	20.0	-2.2	25.7	25.5	.2
3	19.0	18.9	.1	25.7	24.4	+1.3
4	19.3	19.9	-.6	26.0	25.6	.4
5	19.0	20.4	-1.4	25.6	26.3	-.7
6	18.4	19.4	-1.0	25.8	25.9	-.1
7	18.8	18.5	.3	25.6	24.3	+1.3
8	19.8	19.6	.2	25.8	25.2	.6
9	20.8	21.8	-1.0	26.3	25.6	.7
10	^b 21.5	22.4	-.9	^b 26.2	25.5	.7
12	28.1	27.0	+1.1	25.0	24.3	.7
Error mean deviation			-0.52 ‰			0.55° C
Error standard deviation92 ‰			.59° C

^aError equals sea-truth value minus measured value.^bMean of value of several surface measurements.

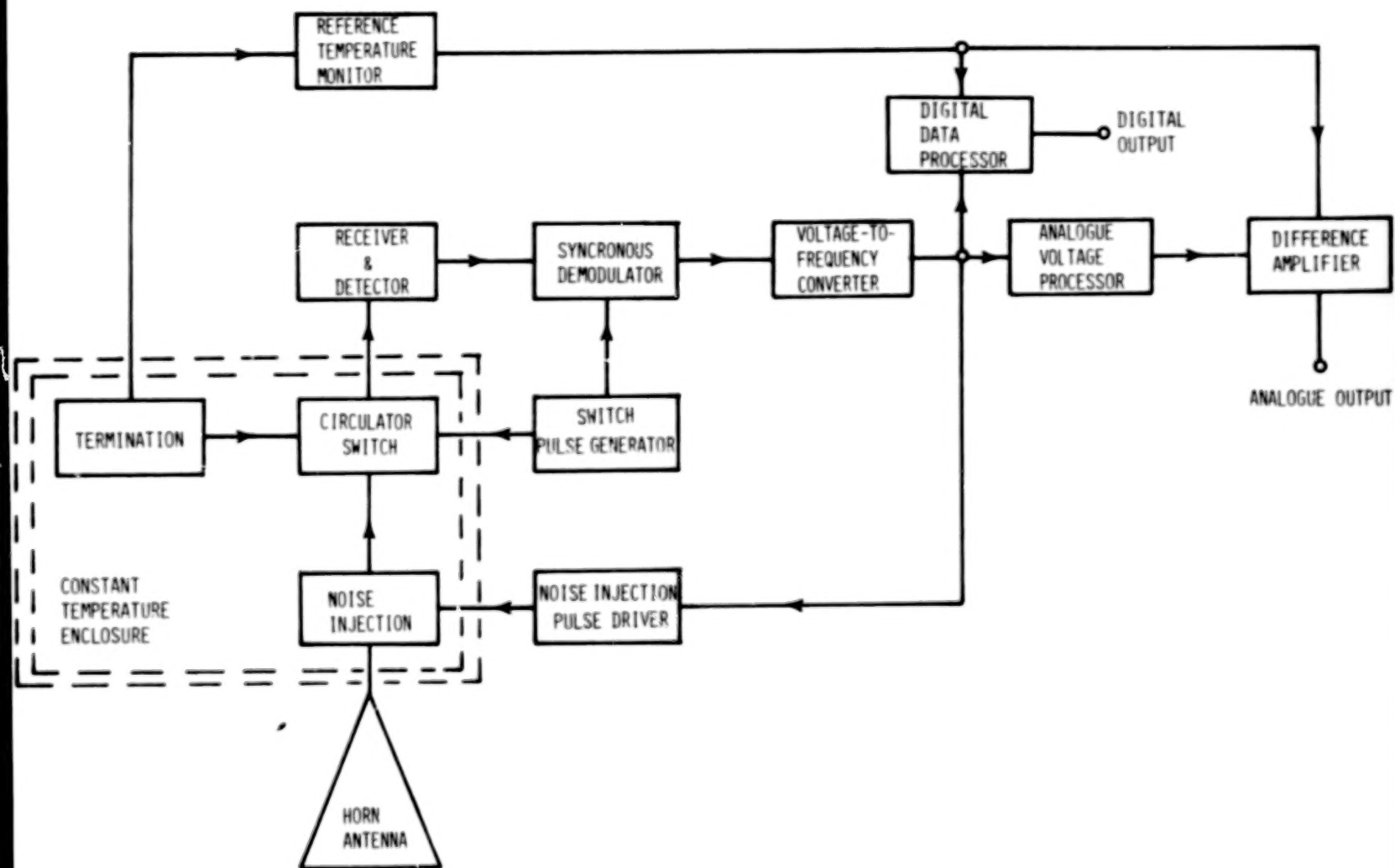


Figure 1.- Simplified block diagram of precision radiometer.

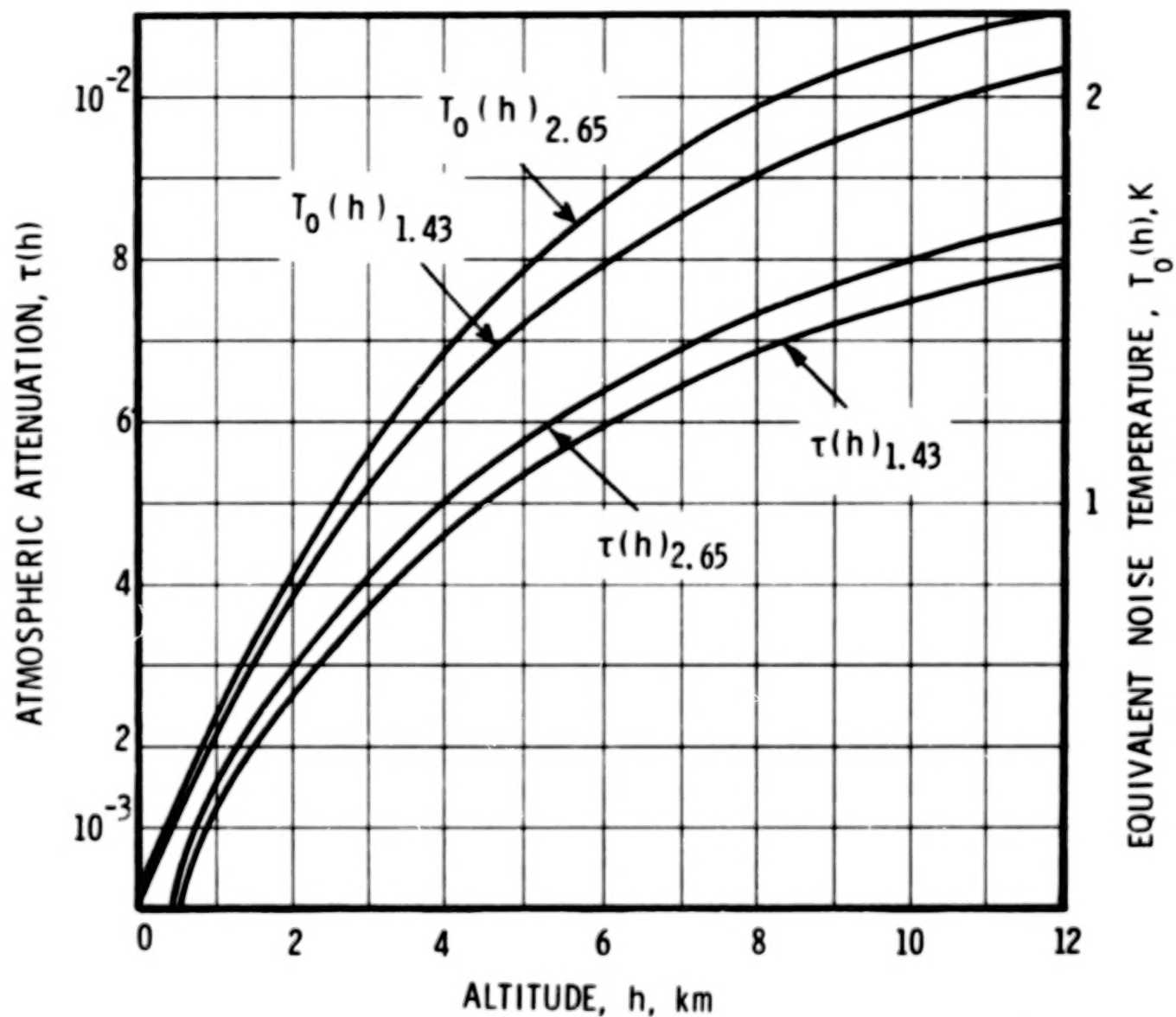


Figure 2.- Atmospheric attenuation and equivalent noise temperature of the 1962 U.S. Standard Atmosphere for different altitudes at 1.43 GHz and 2.65 GHz.

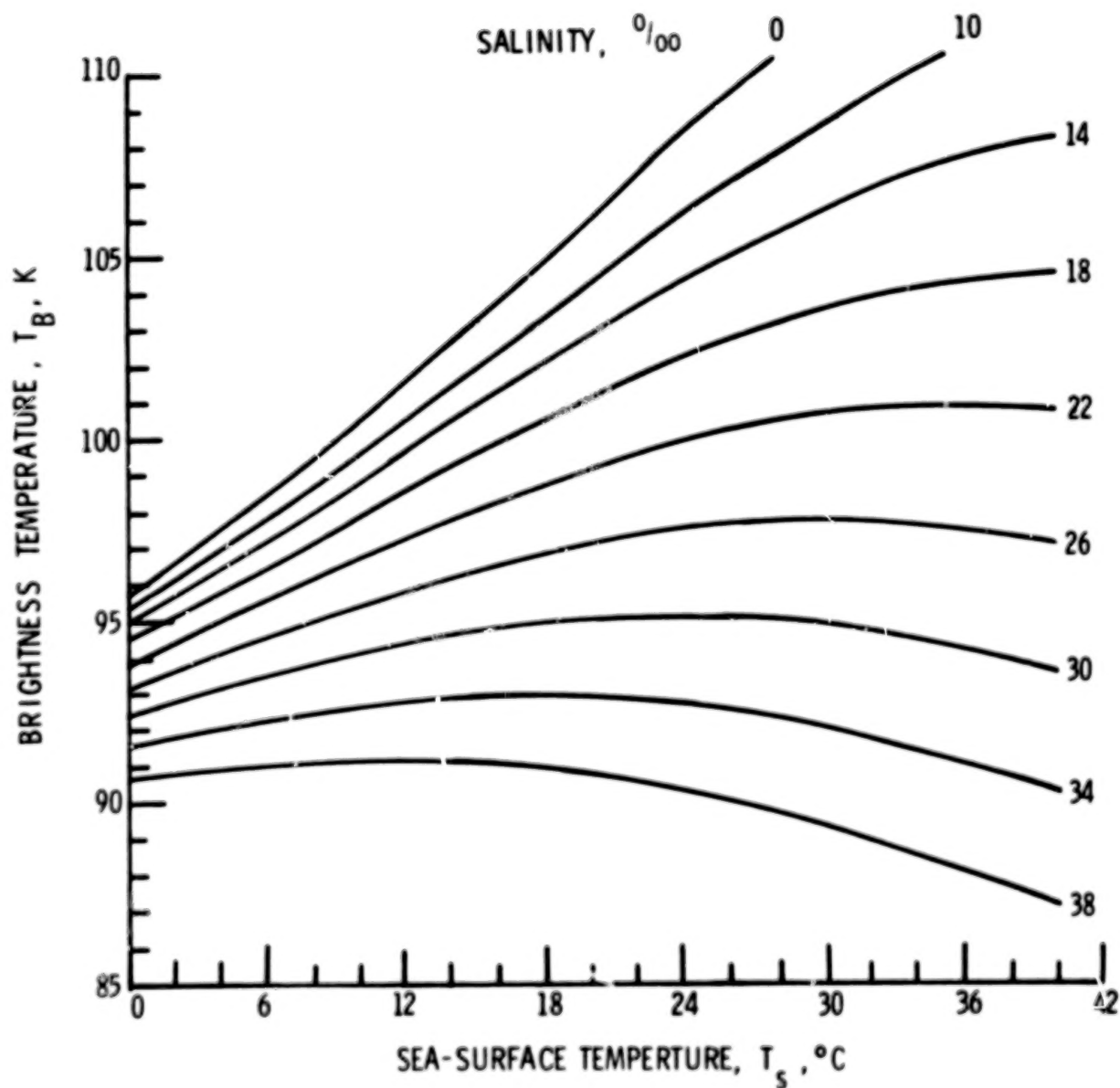


Figure 3.- Brightness temperature at normal incidence versus molecular sea-surface temperature for smooth sea. $f = 1.43$ GHz.

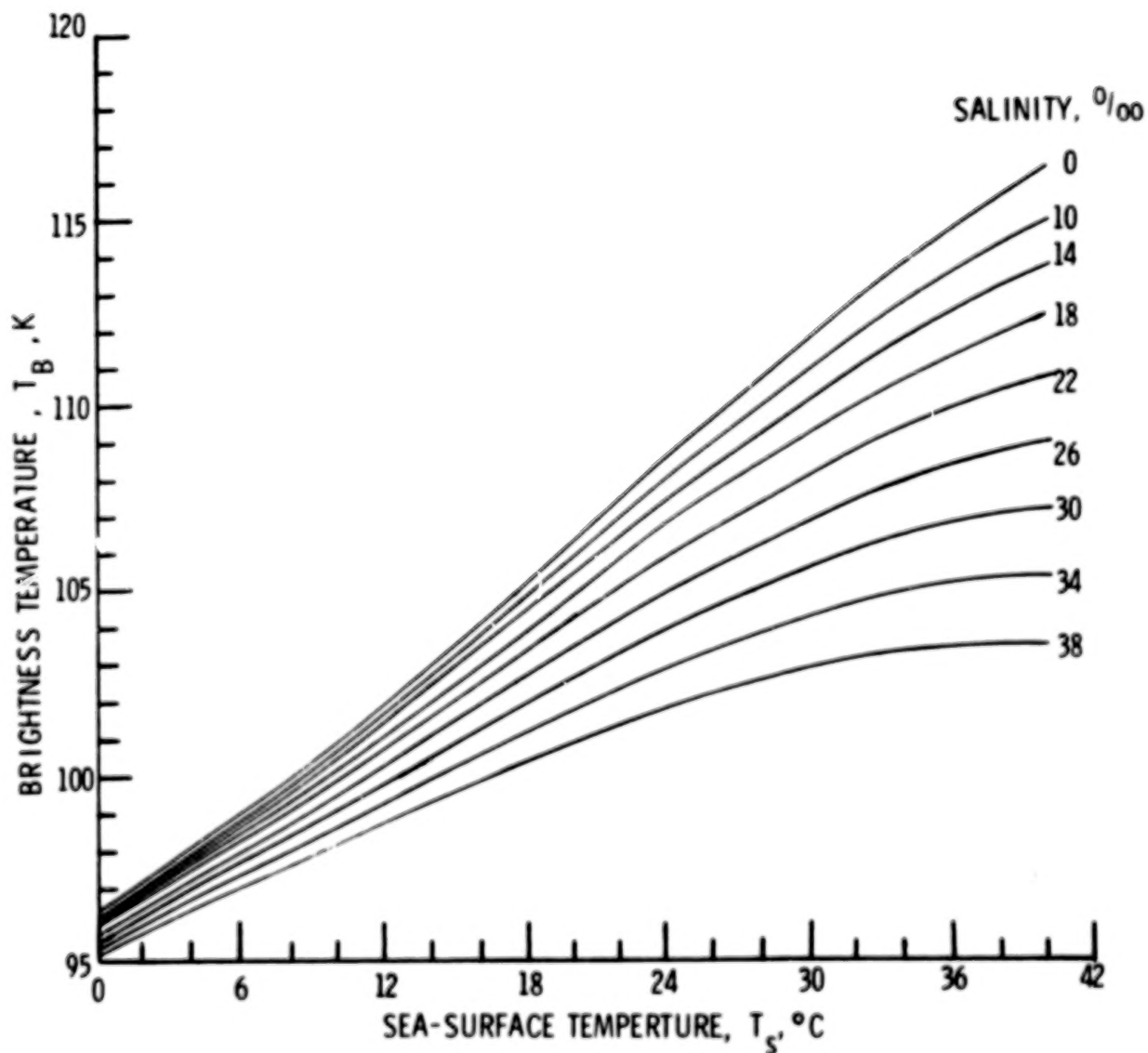


Figure 4.- Brightness temperature at normal incidence versus molecular sea-surface temperature for smooth sea. $f = 2.65$ GHz.

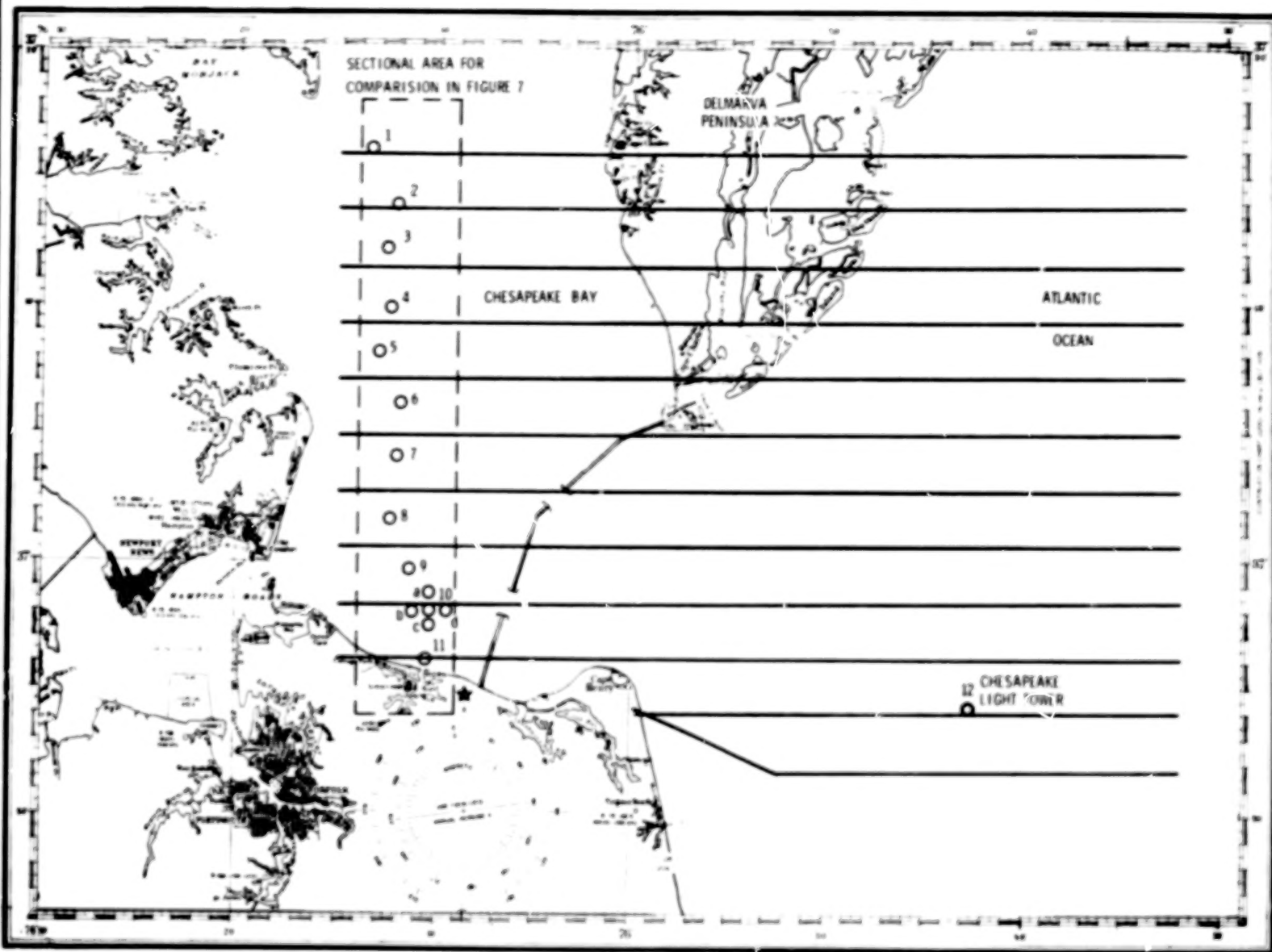


Figure 5.- Flight pattern over the entrance to the Chesapeake Bay and sea-truth locations.

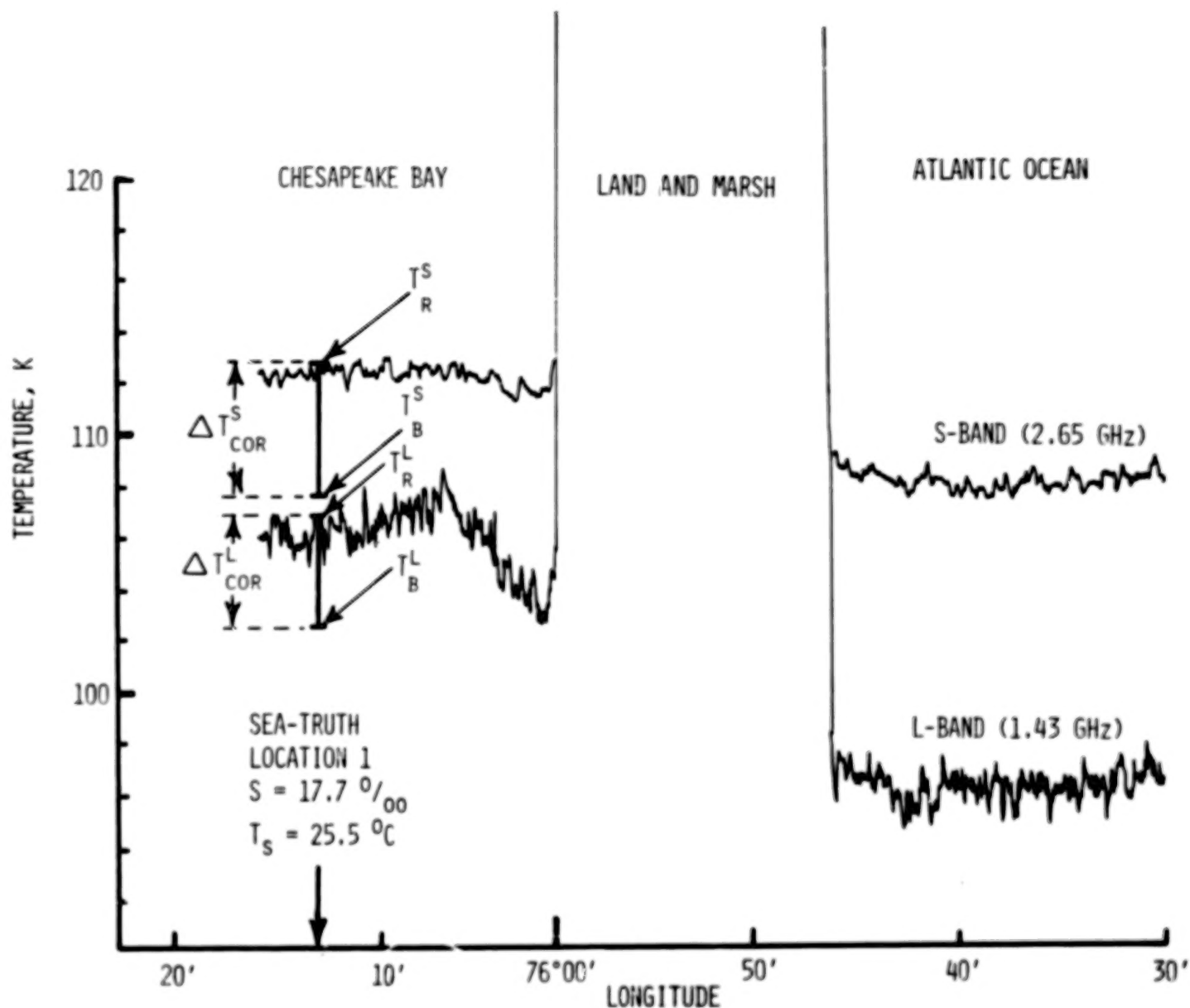


Figure 6.- Raw analogue data record along flight line at $37^{\circ}16'$ latitude.

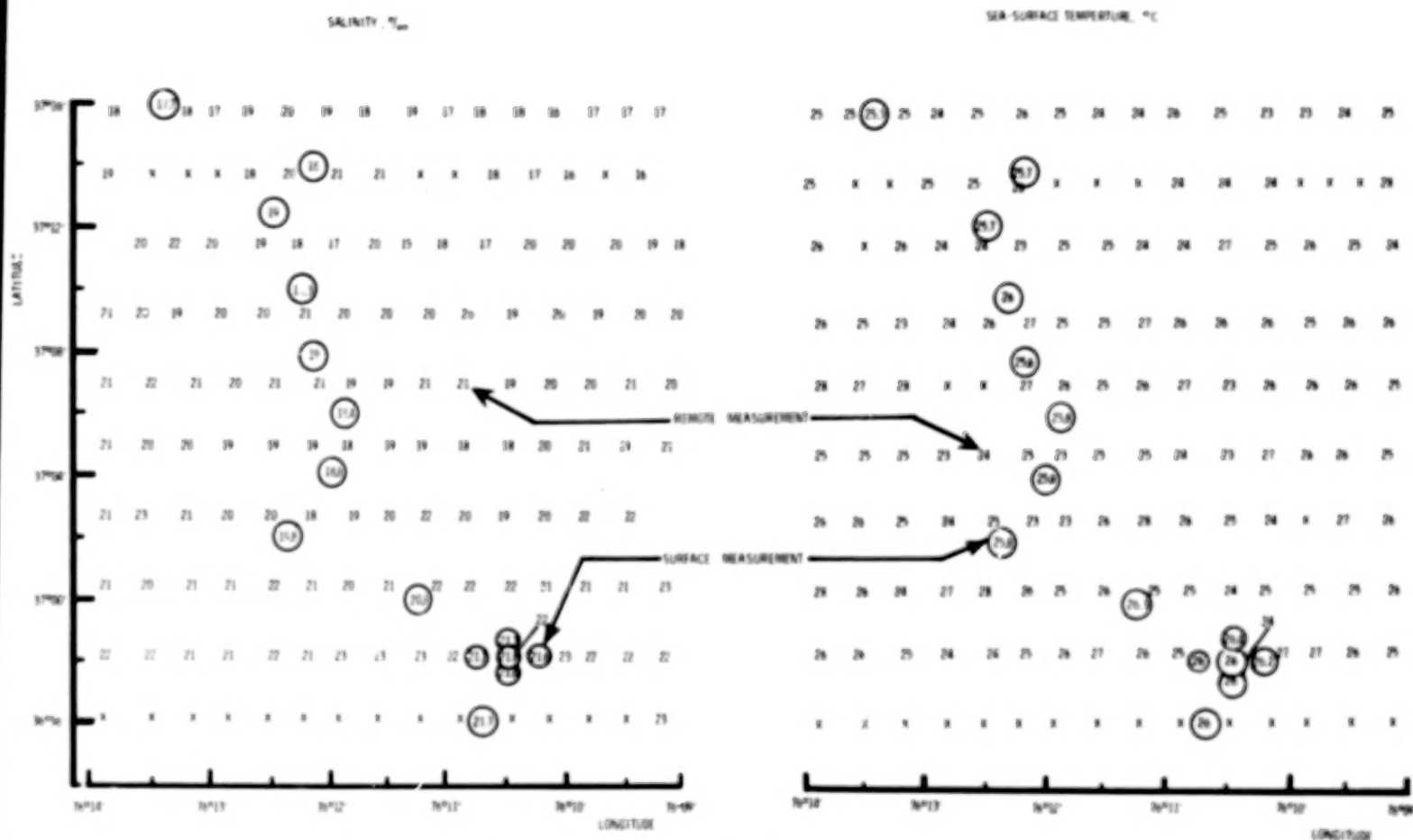


Figure 7.- Comparison of remote measurements of salinity and temperature with surface measurements.

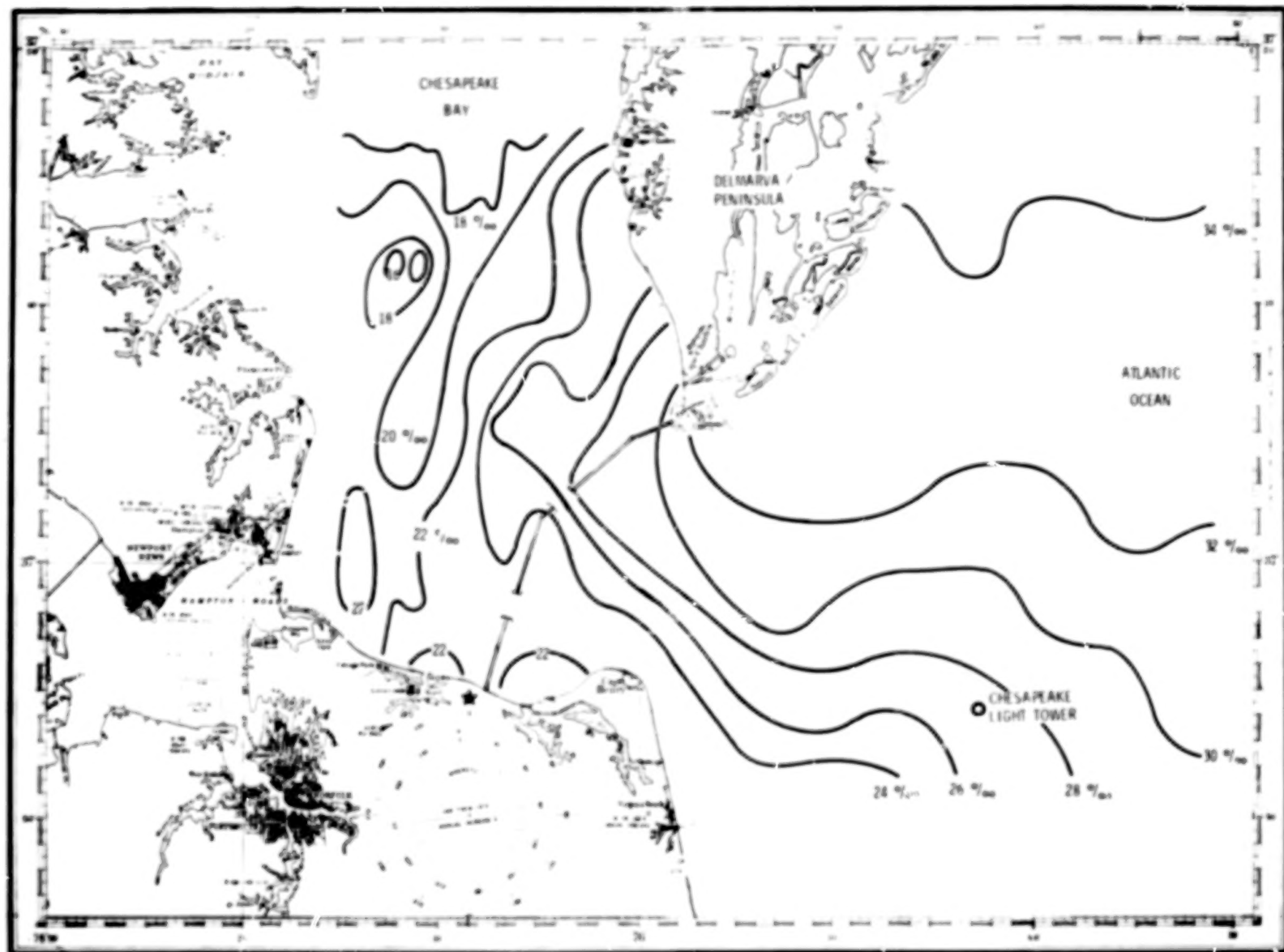


Figure 8.- Isohalines of the lower Chesapeake Bay in 2 ‰ increments on August 24, 1976.

1. Report No. NASA TP-1077		2. Government Accession No.		3. Recipient's Catalog No.	
4. Title and Subtitle SEA-SURFACE TEMPERATURE AND SALINITY MAPPING FROM REMOTE MICROWAVE RADIOMETRIC MEASUREMENTS OF BRIGHTNESS TEMPERATURE				5. Report Date December 1977	
				6. Performing Organization Code	
7. Author(s) Hans-Juergen C. Blume, Bruce M. Kendall, and John C. Fedors				8. Performing Organization Report No. L-11763	
9. Performing Organization Name and Address NASA Langley Research Center Hampton, VA 23665				10. Work Unit No. 175-20-30-01	
				11. Contract or Grant No.	
12. Sponsoring Agency Name and Address National Aeronautics and Space Administration Washington, DC 20546				13. Type of Report and Period Covered Technical Paper	
				14. Sponsoring Agency Code	
15. Supplementary Notes					
16. Abstract <p>A technique to measure remotely sea-surface temperature and salinity was demonstrated with a dual-frequency microwave radiometer system. Accuracies in temperature of 1°C and in salinity of 1 part per thousand (‰) for salinity greater than 5 ‰ were attained after correcting for the influence of extraterrestrial background radiation, atmospheric radiation and attenuation, sea-surface roughness, and antenna beamwidth. The radiometers, operating at 1.43 and 2.65 GHz, comprise a third-generation system using null balancing and feedback noise injection. Flight measurements from an aircraft at an altitude of 1.4 km over the lower Chesapeake Bay and coastal areas of the Atlantic Ocean resulted in contour maps of sea-surface temperature and salinity with a spatial resolution of 0.5 km.</p>					
17. Key Words (Suggested by Author(s)) Salinity Radiometers Sea-surface Remote sensing temperature Brightness Oceanography temperature Microwave				18. Distribution Statement Unclassified - Unlimited Subject Category 48	
19. Security Classif. (of this report) Unclassified		20. Security Classif. (of this page) Unclassified		21. No. of Pages 26	
				22. Price* \$4.50	